Separating surface structure and surface charge with second-harmonic and sum-frequency scattering

Alex G. F. de Beer,[1,*] R. Kramer Campen,[2] and Sylvie Roke[1,†]
[1]*Max Planck Institute for Metals Research, Heisenbergstrasse 3, D70569 Stuttgart, Germany*
[2]*FOM Institute for Atomic and Molecular Physics (AMOLF), Science Park 104, 1098 XG Amsterdam, The Netherlands*
(Received 25 August 2010; published 16 December 2010)

We analyze the effect of an electrostatic surface charge on the angular nonlinear light scattering pattern from spherical particles in solution. An electrostatic field near a charged interface leads to a bulk-allowed third-order process, the strength of which is proportional to the electrostatic surface potential. The commonly isotropic nature of the bulk leads to a fixed angular scattering pattern with fixed intensity ratios between polarizations. We show that second- and third-order scattering effects are separable due to their different angular radiation patterns. Furthermore, nonlinear light scattering from a third-order contribution is strongest in the *ppp* polarization combination.

DOI: 10.1103/PhysRevB.82.235431 PACS number(s): 82.70.Dd, 68.35.B−, 42.65.Ky, 33.20.Tp

I. INTRODUCTION

Colloidal suspensions cover a wide range of technological applications and are responsible for many biological phenomena. Considerable interest exists in the processes that form and stabilize such systems. In a typical colloidal suspension a number of interactions between the suspended particles are present: (1) van der Waals attraction, (2) electroosmotic repulsion due to surface charge, and (3) steric repulsion or chemical interaction due to surface chemistry.[1] Of these three effects, two originate from the surface of the particle. In order to study these surface-induced interactions, it is necessary to obtain information that is specific to the interface. Ideally, we seek a method that characterizes both surface chemistry and surface potential noninvasively.

Soft matter science has greatly benefited from the emergence of nonlinear optical techniques, such as second-harmonic generation (SHG) and sum-frequency generation (SFG), which allows for the noninvasive recording of interface-specific information while eliminating any influences from the surrounding bulk.[2–19] In these techniques, two electromagnetic waves interact in a sample and can undergo a second-order interaction to generate light at the sum of their frequencies. This interaction is forbidden under spatial inversion symmetry. Near the interface, however, this inversion symmetry is broken so that second-harmonic (SH) or sum-frequency (SF) light can be generated exclusively at the interface.

Aqueous interfaces are often charged, either from excess charge at the interface or ionic adsorbents, so that a strong electrostatic field is present near such interfaces. This electrostatic field may act as a third input field of frequency zero.[20,21] Eisenthal and coworkers[7,22–27] realized that the resulting third-order sum-frequency process is bulk allowed and leads to a signal that is proportional to the electrostatic potential at the interface.

Recently, nonlinear light scattering (NLS) has emerged as a noninvasive tool to probe the interfaces of particles in suspension. Second-order particle surface spectroscopy was pioneered in the Eisenthal group,[28–36] and later extended to record the vibrational spectrum of the interface using sum-frequency scattering.[37–42,67] Like reflection mode SHG and SFG, NLS is sensitive to both surface structure and surface potential.[31,43–45]

Though the first NLS experiments were conducted by capturing the signal in a wide angle behind the sample, it was later recognized that the angular distribution of the scattered signal adds a degree of freedom,[33,37,40,46–49,67] which contains information on particle size and surface structure.[49,50,67] The general properties of the angular scattering pattern have been documented for small particles,[51–53] aqueous suspensions,[37,50,53,54] suspensions with a strong index contrast,[49,52,54,55] and for nonspherical particles.[56,57] The angular scattering pattern that is expected from a third-order ($\boldsymbol{\chi}^{(3)}$) process, however, has never been treated. The angular scattering pattern of a nonlinear process depends on the relative strength of the involved susceptibility components. Since special symmetry relations hold for the $\boldsymbol{\chi}^{(3)}$ process, we can also expect special relationships to hold for the angular scattering pattern.

In this paper we show that NLS simultaneously yields information on surface chemistry and surface potential. These two contributions may be separated by means of the angular scattering pattern when surface and bulk susceptibilities are sufficiently different. The structure of this paper is as follows: first, we review the molecular origin of the second-order surface signal and the third-order potential-dependent signal. We then show that three phenomena may lead to a nonlinear signal: (1) Asymmetry in molecular orientation, typically at the interface, leads to a direct second-order process. (2) Bulk molecules may undergo a third-order process regardless of orientation. (3) Molecular reorientation under the influence of an electric field may lead to an asymmetric orientation distribution in the bulk, and therefore to a second-order interaction.

This last interaction behaves as a third-order interaction since three fields linearly influence the strength of the response. We illustrate the similarity between the second and third effects, and show under what circumstances these two effects may be separated from the first effect. Finally, we derive the angular scattering pattern arising from a third-order process for spherical particles. We show that this pat-

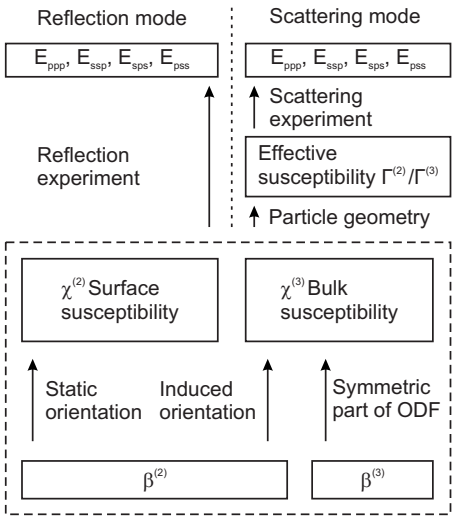

FIG. 1. Relation between detected nonlinear signal (top) and molecular structure (bottom) through molecular orientation and experimental geometry. An asymmetry in the orientation distribution function (ODF) of a molecular layer that is independent of electrostatic field strength leads to a contribution of the second-order hyperpolarizability $\boldsymbol{\beta}^{(2)}$ to the second-order susceptibility $\boldsymbol{\chi}^{(2)}$. When the electrostatic field causes molecular alignment, this may lead to a contribution of $\boldsymbol{\beta}^{(2)}$ to the third-order nonlinear susceptibility $\boldsymbol{\chi}^{(3)}$. Also, the contribution of the third-order hyperpolarizability $\boldsymbol{\beta}^{(3)}$ to $\boldsymbol{\chi}^{(3)}$ is present, even when the ODF is isotropic. In reflection mode, $\boldsymbol{\chi}^{(2)}$ and $\boldsymbol{\chi}^{(3)}$ are probed directly. In scattering mode, however, the overall nonlinear response is determined both by the surface susceptibility and the surface shape of the particle. Both effects are included in the effective particle susceptibility $\boldsymbol{\Gamma}^{(2)}/\boldsymbol{\Gamma}^{(3)}$, which is probed in scattering mode. In a scattering experiment, an extra experimental degree of freedom is present in the form of the angular intensity distribution of scattered light.

tern has a fixed shape, with intensity maxima that only depend on the size of the scattering particle. Thus, it is possible to find angular ranges in which either second- or third-order contributions dominate, thereby optimizing the relative signal strength.

II. NONLINEAR SIGNAL ORIGINS

In this section, we discuss the origin of SH or SF signal from aqueous colloidal suspensions. Fig. 1 shows a diagram connecting the molecular origin of the SH or SF signal (at the bottom of the diagram) to the eventual detected signal (at the top of the diagram).

Starting at the bottom of Fig. 1, at the surface of a suspended particle, symmetry breaking leads to a nonvanishing second-order susceptibility $\boldsymbol{\chi}^{(2)}$ (arrow connecting $\boldsymbol{\beta}^{(2)}$ to $\boldsymbol{\chi}^{(2)}$). The value of $\boldsymbol{\chi}^{(2)}$ depends on the molecular hyperpolarizability $\boldsymbol{\beta}^{(2)}$ and the amount of molecular ordering at the interface. The more profound the breaking of inversion symmetry at the interface is, the larger the value of $\boldsymbol{\chi}^{(2)}$ will be.

The presence of charge at the surface of the particle leads to an electrostatic field projecting into the surrounding medium. Such a field may break the inversion symmetry of the surrounding bulk in two possible ways: First, the field disturbs the electron distribution of the molecules in the medium, leading to an interaction through the third-order hyperpolarizability $\boldsymbol{\beta}^{(3)}$ (indicated in Fig. 1 by the arrow connecting $\boldsymbol{\beta}^{(3)}$ to $\boldsymbol{\chi}^{(3)}$). Second, a mechanical reorientation of the molecules in the medium may occur,[21] through the interaction of the electric field with the molecules' permanent molecular dipole moment. Such a reorientation leads to a bulk ordering, and gives rise to an indirect contribution to the third order susceptibility $\boldsymbol{\chi}^{(3)}$, which depends on the second-order hyperpolarizability $\boldsymbol{\beta}^{(2)}$ (indicated in Fig. 1 by the arrow connecting $\boldsymbol{\beta}^{(2)}$ to $\boldsymbol{\chi}^{(3)}$). We show that both the direct (via $\boldsymbol{\beta}^{(3)}$) and indirect (via $\boldsymbol{\beta}^{(2)}$) bulk effects scale linearly with the electrostatic field and thus the surface potential.

Further up in the block diagram of Fig. 1, the two susceptibilities $\boldsymbol{\chi}^{(2)}$ and $\boldsymbol{\chi}^{(3)}$ contain information on surface chemistry and surface charge, respectively. In a reflection mode experiment individual elements of the $\boldsymbol{\chi}^{(2)}$ and $\boldsymbol{\chi}^{(3)}$ tensors can be selected by polarization (indicated by the arrow denoted by "reflection experiment"). In these experiments, light is collected in the direction for which the reflected source beams are phase matched with the nonlinear signal. In a scattering mode experiment, however, the limited size of the suspended particle leads to a broad angular scattering pattern. This angular scattering pattern adds an additional experimental degree of freedom. In Sec. III, we treat the formalism for nonlinear light scattering from a suspension of small, spherical, particles. Every particle has an effective particle susceptibility that is a function of the susceptibility of its surface (the dashed box in Fig. 1) and of the shape of the particle. In scattering mode, these susceptibilities can also be probed by selecting different polarization combinations (indicated by the arrow denoted "scattering experiment" in Fig. 1). We derive expressions for the angular scattering patterns of both the second-order, surface specific effect and the third-order, potential-dependent effect.

Molecular origin of SF and SH signals

In SHG and SFG, the (surface) nonlinear response is typically described in terms of a nonlinear polarization. The full nonlinear polarization is an expansion starting with a second-order $\mathbf{P}^{(2)}$ and third-order $\mathbf{P}^{(3)}$ polarization, followed by higher order terms,

$$\mathbf{P}_{NL}(\omega_0) = \mathbf{P}^{(2)}(\omega_0) + \mathbf{P}^{(3)}(\omega_0) + \cdots, \tag{1}$$

$$\mathbf{P}^{(2)}(\omega_0 = \omega_1 + \omega_2) = \epsilon_0 \boldsymbol{\chi}^{(2)} : \mathbf{E}_1(\omega_1)\mathbf{E}_2(\omega_2), \tag{2}$$

$$\mathbf{P}^{(3)}(\omega_0 = \omega_1 + \omega_2) = \epsilon_0 \boldsymbol{\chi}^{(3)} : \mathbf{E}_1(\omega_1)\mathbf{E}_2(\omega_2)\mathbf{E}_3(\omega_3 = 0), \tag{3}$$

where $\boldsymbol{\chi}^{(2)}$ and $\boldsymbol{\chi}^{(3)}$ are the second-order and third-order susceptibility terms, respectively. Though the source fields $\mathbf{E}_{1,2,3}$ can be any combination of electric fields, here we limit ourselves to the nonlinear polarization oscillating at the sum of the frequency of two source fields, $\mathbf{E}_1$ and $\mathbf{E}_2$. For the third field $\mathbf{E}_3$ we take an electrostatic field $\mathbf{E}_{dc}$, which does not modify the sum of the frequencies. It should be noted that for a SH process, $\mathbf{E}_1$ and $\mathbf{E}_2$ are degenerate. The second-order

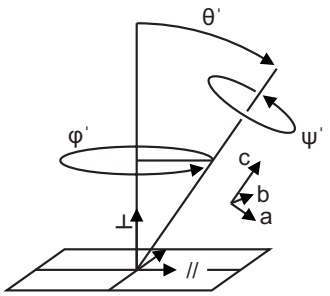

FIG. 2. Illustration of the coordinate transformation from the molecular coordinate system (a,b,c) to the surface coordinate system defined by a perpendicular ($\perp$) and two parallel ($\parallel$) directions. Every molecule has an orientation given by (1) a rotation around the molecular c axis by an angle ψ', (2) a tilt by an angle θ', and (3) a rotation around the interfacial normal direction ($\perp$) by an angle ϕ'. Each set of three rotation angles uniquely defines a molecular orientation.

susceptibility $\boldsymbol{\chi}^{(2)}$ is nonzero only if inversion symmetry is broken. In many experiments, this only takes place at the interface of a particle so that $\boldsymbol{\chi}^{(2)}$ contains information on surface chemistry and structure. The third-order process is allowed even for an isotropic bulk; the amplitude of the contribution scales with the surface potential and the magnitude of the third-order susceptibility. In the following section, we use the orientation distribution function (ODF) of molecules near an interface to describe the second- and third-order susceptibilities near a particle surface.

1. Second-order susceptibility and the ODF

The nonlinear susceptibilities $\boldsymbol{\chi}^{(2)}$ and $\boldsymbol{\chi}^{(3)}$ are material properties. The second-order contribution depends on the molecular hyperpolarizability $\boldsymbol{\beta}^{(2)}$, the density of molecules and their orientation distribution according to

$$\chi^{(2)}_{ijk} = \sum_{a,b,c} T_{ia}T_{jb}T_{kc}\beta^{(2)}_{abc} = N_m\langle T_{ia}T_{jb}T_{kc}\rangle\beta^{(2)}_{abc}, \tag{4}$$

where N_m is the molecular density at the interface and $\mathbf{T}$ is the matrix that transforms from a coordinate system (a,b,c), relative to the molecular axes, to the macroscopic coordinate system of $\boldsymbol{\chi}^{(2)}$, relative to the surface normal of an interface. We use $\perp$ to denote the surface normal direction and $\parallel$ to denote the direction along the surface. As an example of the transformation of Eq. (4), the contribution of $\beta^{(2)}_{ccc}$ to $\chi^{(2)}_{\perp\perp\perp}$ is given by $N_m\langle\cos^3\theta'\rangle$, with θ' the angle between the c axis (e.g., a symmetry axis) of the molecule and the $\perp$ axis of the macroscopic coordinate system (e.g., a surface normal).

The average transformation $\langle T_{ia}T_{jb}T_{kc}\rangle$ depends on the ODF of the molecules for which $\boldsymbol{\chi}^{(2)}$ is calculated. The ODF $p(\psi',\theta',\phi')$ describes the probability density of finding a molecule rotated by Euler angles ψ', θ', and ϕ'. Figure 2 shows an illustration of the coordinate transform from the molecular coordinate frame (a,b,c) to the surface coordinate frame given by a perpendicular ($\perp$) and two parallel directions ($\parallel$). The Euler angles describe an angle of rotation around the c axis of a molecule (ψ'), a tilt angle between the c axis of a molecule and the $\perp$ axis of the macroscopic coordinate system (θ') and a rotation around the $\perp$ axis of the macroscopic coordinate system (ϕ'). Throughout this paper, we assume a rotationally isotropic interface (i.e., isotropic with respect to ϕ') and nonchiral molecules both at the interface and in the bulk. Furthermore, we assume that all molecules are isotropically distributed with respect to ψ'. Under these assumptions, the ODF is exclusively a function of the tilt angle θ' . We can write such an ODF as an expansion of Legendre polynomials P_n,

$$p(\psi',\theta',\phi') = p(\theta') = \sin\theta'\sum_{n=0}^{\infty}\frac{(2n+1)}{2}w_nP_n(\cos\theta'), \tag{5}$$

here, the w_n are weights of the terms of the expansion. If p is normalized, $w_0=1$. In this expansion, the even orders (order 0, 2, 4, etc.) are the inversion symmetric contributions and the odd orders (order 1, 3, 5, etc.) are the inversion asymmetric contributions to the ODF. Even orders therefore contribute exclusively to inversion symmetry allowed processes, such as the bulk-allowed $\boldsymbol{\chi}^{(3)}$ process, while odd orders contribute exclusively to inversion symmetry forbidden processes, such as the $\boldsymbol{\chi}^{(2)}$ process. Values for w_n can be extracted from an ODF using

$$w_n = \int p(\theta')P_n(\cos\theta')\sin\theta'd\theta'. \tag{6}$$

Every expansion order n corresponds[58–61] to an irreducible tensor $\mathbf{A}_n$, so that $\boldsymbol{\chi}$ becomes a linear combination of these tensors, weighted by the values of w_n. Furthermore, the number of nonvanishing irreducible tensors is limited by the rank of $\boldsymbol{\chi}$, which is 3 for a $\boldsymbol{\chi}^{(2)}$ process and 4 for a $\boldsymbol{\chi}^{(3)}$ process. It is therefore sufficient to have knowledge of w_1 and w_3 to completely predict the value of the $\boldsymbol{\chi}^{(2)}$ tensor, and knowledge of w_0, w_2, and w_4 is sufficient to describe $\boldsymbol{\chi}^{(3)}$.

The second-order susceptibility $\boldsymbol{\chi}^{(2)}$, is a linear combination of $\mathbf{A}^{(2)}_1$ and $\mathbf{A}^{(2)}_3$,

$$\boldsymbol{\chi}^{(2)} = N_m(w_1\mathbf{A}^{(2)}_1 + w_3\mathbf{A}^{(2)}_3) \tag{7}$$

for which w_1 and w_3 take the form

$$w_1 = \int p(\theta')\cos\theta'\sin\theta'd\theta', \tag{8}$$

$$w_3 = \int p(\theta')\left(\frac{5}{2}\cos^3\theta' - \frac{3}{2}\cos\theta'\right)\sin\theta'd\theta'. \tag{9}$$

The first weight w_1 may be interpreted as the overall asymmetry of an ODF, and is identical to the term $\langle\cos\theta'\rangle$ found in many publications (for a review, see Ref. 62). The weight w_3 indicates the additional "sharpness" of a distribution. For very broad distributions, the value of w_3 will be close to zero. Since P_3 is zero for $\theta'=39.2°$, a broad distribution is indistinguishable[63] from a distribution that is sharply peaked around 39.2° since for such a distribution w_3 will vanish as well.

The tensors $\mathbf{A}^{(2)}_1$ and $\mathbf{A}^{(2)}_3$ depend on $\boldsymbol{\beta}^{(2)}$ in the following way:

TABLE I. Overview of the shorthand notation for independent tensor components used in this work. Shown here are the definitions for $\boldsymbol{\chi}^{(2)}$. The choice is convenient since $\chi_1^{(2)}$ is dependent only on w_3. Definitions for $\boldsymbol{\chi}^{(3)}$, $\boldsymbol{\Gamma}^{(2)}$, and $\boldsymbol{\Gamma}^{(3)}$ can be obtained by replacing with the appropriate symbols.

Indexed component	Tensor components	Depends on
$\chi_1^{(2)}$	$\chi^{(2)}_{\perp\perp\perp}-\chi^{(2)}_{\parallel\parallel\perp}-\chi^{(2)}_{\parallel\perp\parallel}-\chi^{(2)}_{\perp\parallel\parallel}$	w_3
$\chi_2^{(2)}$	$\chi^{(2)}_{\parallel\parallel\perp}$	w_1, w_3
$\chi_3^{(2)}$	$\chi^{(2)}_{\parallel\perp\parallel}$	w_1, w_3
$\chi_4^{(2)}$	$\chi^{(2)}_{\perp\parallel\parallel}$	w_1, w_3

$$\mathbf{A}^{(2)}_{1,ijk} = a_{1,1}\delta_{ij}\delta_{k\perp} + a_{1,2}\delta_{ik}\delta_{j\perp} + a_{1,3}\delta_{jk}\delta_{i\perp}, \tag{10}$$

$$a_{1,1} = \sum_{ijk} \beta^{(2)}_{ijk}(4\delta_{ij}\delta_{kc} - \delta_{ik}\delta_{jc} - \delta_{jk}\delta_{ic})/10$$

$$= \frac{1}{10}(4\beta^{(2)}_{aac} + 4\beta^{(2)}_{bbc} + 2\beta^{(2)}_{ccc} - \beta^{(2)}_{aca} - \beta^{(2)}_{bcb} - \beta^{(2)}_{caa} - \beta^{(2)}_{cbb}), \tag{11}$$

$$a_{1,2} = \sum_{ijk} \beta^{(2)}_{ijk}(4\delta_{ik}\delta_{jc} - \delta_{jk}\delta_{ic} - \delta_{ij}\delta_{kc})/10, \tag{12}$$

$$a_{1,3} = \sum_{ijk} \beta^{(2)}_{ijk}(4\delta_{jk}\delta_{ic} - \delta_{ij}\delta_{kc} - \delta_{ik}\delta_{jc})/10, \tag{13}$$

$$\mathbf{A}^{(2)}_{3,ijk} = a_3\left[\frac{5}{2}\delta_{iz}\delta_{jz}\delta_{kz} - \frac{1}{2}(\delta_{ij}\delta_{kz} + \delta_{ik}\delta_{jz} + \delta_{jk}\delta_{iz})\right], \tag{14}$$

$$a_3 = \frac{1}{5}(2\beta^{(2)}_{ccc} - \beta^{(2)}_{aac} - \beta^{(2)}_{bbc} - \beta^{(2)}_{aca} - \beta^{(2)}_{bcb} - \beta^{(2)}_{caa} - \beta^{(2)}_{cbb}), \tag{15}$$

where $\delta_{ij}=1$ for $i=j$, and zero otherwise so that, for instance, $A^{(2)}_{1,\perp\perp\perp} = a_{1,1}+a_{1,2}+a_{1,3} = A^{(2)}_{1,\parallel\parallel\perp} + A^{(2)}_{1,\parallel\perp\parallel} + A^{(2)}_{1,\perp\parallel\parallel}$. The characters $a_{1,n}$ and a_3 denote tensor invariants,[59] which are linear combinations of the components of $\boldsymbol{\beta}^{(2)}$.

The second-order surface susceptibility therefore generally has four independent components. It is convenient to define $\chi_1^{(2)}$ as the difference between $\chi^{(2)}_{\perp\perp\perp}$ and $\chi^{(2)}_{\parallel\parallel\perp} + \chi^{(2)}_{\parallel\perp\parallel} + \chi^{(2)}_{\perp\parallel\parallel}$ and $\chi^{(2)}_{2,3,4}$ as each of the latter three components, respectively. Such a definition leads to simplified, more insightful expressions. For instance, $\chi_1^{(2)}$ can be nonzero only when w_3 is nonzero. Table I shows the definitions for the indexed $\boldsymbol{\chi}^{(2)}$, $\boldsymbol{\chi}^{(3)}$, and $\boldsymbol{\Gamma}^{(2)}$ components we use throughout this paper.

2. Third-order susceptibility and the ODF

Even though $\boldsymbol{\beta}^{(3)}$ is an estimated seven order of magnitude smaller[64] than $\boldsymbol{\beta}^{(2)}$, this difference in magnitude may be compensated by the fact that the second-order signal originates solely from molecules at the interface while the third-order signal is bulk allowed and has a far greater number of molecules contributing to it. Thus, in the presence of an electrostatic field, the third-order signal may reach amplitudes that are comparable to the second-order amplitude. Here, we consider a bulk consisting of molecules with an (initially) isotropic orientation ($w_0=1$, all other weights zero).

It is important to note that an electrostatic field leads to a third-order nonlinear response by two different pathways: (1) a pure third-order interaction that is the result of the interaction of source waves $\mathbf{E}_1$ and $\mathbf{E}_2$ with the electrostatic field $\mathbf{E}_{\mathrm{dc}}$, the strength of which is determined by the third-order hyperpolarizability $\boldsymbol{\beta}^{(3)}$ and (2) an indirect interaction that is the result of the electrostatic field acting on the permanent electrostatic dipole of the water molecule. The electrostatic field causes a mechanical realignment of the molecules, which breaks inversion symmetry. Even though this latter contribution is determined by the value of $\boldsymbol{\beta}^{(2)}$, both of these contributions depend (linearly) on three input fields, and may therefore be regarded as third-order processes.

The part proportional to $\boldsymbol{\beta}^{(3)}$ is given by

$$\chi^{(3)}_{ijkl} = \mathbf{A}^{(3)}_{0,ijkl} = a_{0,1}\delta_{ij}\delta_{kl} + a_{0,2}\delta_{il}\delta_{jk} + a_{0,3}\delta_{ik}\delta_{jl}, \tag{16}$$

$$a_{0,1} = \sum_{ijkl} \beta^{(3)}_{ijkl}(4\delta_{ij}\delta_{kl} - \delta_{ik}\delta_{jl} - \delta_{il}\delta_{jk})/30, \tag{17}$$

$$= \frac{1}{30}(4\beta^{(3)}_{aabb} + 4\beta^{(3)}_{aacc} + 4\beta^{(3)}_{bbaa} + 4\beta^{(3)}_{bbcc} + 4\beta^{(3)}_{ccaa} + 4\beta^{(3)}_{ccbb} + 2\beta^{(3)}_{aaaa} + 2\beta^{(3)}_{bbbb} + 2\beta^{(3)}_{cccc} - \beta^{(3)}_{abab} - \beta^{(3)}_{acac} - \beta^{(3)}_{baba} - \beta^{(3)}_{bcbc} - \beta^{(3)}_{caca} - \beta^{(3)}_{cbcb} - \beta^{(3)}_{baab} - \beta^{(3)}_{caac} - \beta^{(3)}_{abba} - \beta^{(3)}_{cbbc} - \beta^{(3)}_{acca} - \beta^{(3)}_{bccb}), \tag{18}$$

$$a_{0,2} = \sum_{ijkl} \beta^{(3)}_{ijkl}(4\delta_{il}\delta_{jk} - \delta_{ij}\delta_{kl} - \delta_{ik}\delta_{jl})/30, \tag{19}$$

$$a_{0,3} = \sum_{ijkl} \beta^{(3)}_{ijkl}(4\delta_{ik}\delta_{jl} - \delta_{ij}\delta_{kl} - \delta_{il}\delta_{jk})/30, \tag{20}$$

which is similar to $\mathbf{A}_1^{(2)}$ and shares the symmetry rule $A_{0,\perp\perp\perp\perp} = A_{0,\parallel\parallel\perp\perp} + A_{0,\parallel\perp\parallel\perp} + A_{0,\perp\parallel\parallel\perp}$.

The second contribution, which is caused by the reorientation of molecules, depends on the torque exerted on the molecules by the electrostatic field. For a liquid that has an isotropic ODF for $\mathbf{E}_{\mathrm{dc}}=0$, the ODF under the influence of an electrostatic field will resemble a Boltzmann distribution driven by the electrostatic energy,[21,65] $\boldsymbol{\mu}_{\mathrm{dc}}\cdot\mathbf{E}_{\mathrm{dc}}$,

$$p(\theta') = \frac{m_{\mathrm{dc}}E_{\mathrm{dc}}}{\sinh(m_{\mathrm{dc}}E_{\mathrm{dc}})} e^{m_{\mathrm{dc}}E_{\mathrm{dc}}\cos\theta'} \sin\theta'$$

$$= \frac{\sin\theta'}{2}(1 + m_{\mathrm{dc}}E_{\mathrm{dc}}\cos\theta' + O[(m_{\mathrm{dc}}E_{\mathrm{dc}})^2]), \tag{21}$$

where $m_{\mathrm{dc}} = \mu_{\mathrm{dc}}/k_BT$, μ_{dc} is the permanent dipole moment of the molecule and k_BT is the product of the Boltzmann constant with absolute temperature. The factor $\sinh(m_{\mathrm{dc}}E_{\mathrm{dc}})$ normalizes the distribution. The product $m_{\mathrm{dc}}E_{\mathrm{dc}}$ is generally

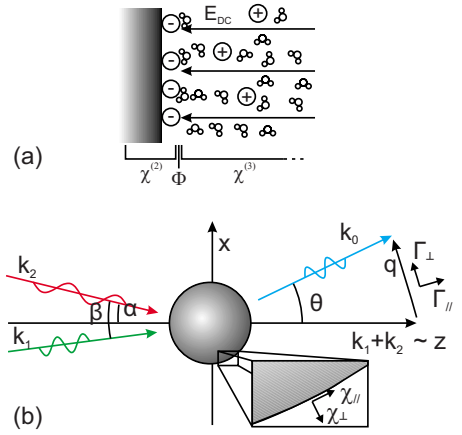

FIG. 3. (Color online) (a) Cartoon of a charged interface in contact with an aqueous electrolyte solution. Negative ions adsorbed at the surface cause an electric field (arrows) which attracts counter-ions and repels co-ions. Symmetry breaking near the charged interface results in a contribution from $\boldsymbol{\chi}^{(2)}$. The signal arising from $\boldsymbol{\chi}^{(3)}$ is proportional to E_{dc} and bulk allowed. Integration of the $\boldsymbol{\chi}^{(3)}$ signal over all space gives the potential Φ near the interface. (b) Overview of nonlinear light scattering: two electromagnetic waves with wave vectors $\mathbf{k}_1$ and $\mathbf{k}_2$ create a nonlinear polarization at or near the interface of a particle, which is centered at the origin. A nonlinear scattering pattern is emitted and detected at an angle θ with respect to a forward direction defined by $\mathbf{k}_1+\mathbf{k}_2$. The wave vector of the detected field is $\mathbf{k}_0$, and the scattering vector $\mathbf{q}$ is defined as $\mathbf{q}=\mathbf{k}_0-\mathbf{k}_1-\mathbf{k}_2$. The opening angle β is the angle between $\mathbf{k}_1$ and $\mathbf{k}_2$ while α defines the angle between $\mathbf{k}_2$ and the forward direction. In a second-harmonic scattering experiment, $\mathbf{k}_1$ and $\mathbf{k}_2$ are degenerate.

lower than unity. For example, for the product to exceed 1 in water, E_{dc} has to exceed 10^9 V m^{-1}, an electric field strength that is generally only found within the first hydration layer of water around an ion. For all other circumstances, $\mu_{\mathrm{dc}}E_{\mathrm{dc}}/k_BT \ll 1$, so that all higher order terms in Eq. (21) are negligible. An electrostatic field therefore induces an ODF with $w_1 \propto E_{\mathrm{dc}}$. This reorientation then results in a second-order (i.e., determined by $\boldsymbol{\beta}^{(2)}$) process. For an electrostatic field pointing along the normal direction of an interface, the final expression for $\boldsymbol{\chi}^{(3)}$ then becomes[24]

$$\chi^{(3)}_{ijk,\perp}E_{\mathrm{dc},\perp} = w_0 A^{(3)}_{0,ijk,\perp}E_{\mathrm{dc},\perp} + w_1(E_{\mathrm{dc},\perp})A^{(2)}_{1,ijk}$$

$$= A^{(3)}_{0,ijk,\perp}E_{\mathrm{dc},\perp} + \frac{2\mu_{\mathrm{dc}}}{3k_BT}A^{(2)}_{1,ijk}E_{\mathrm{dc},\perp}, \qquad (22)$$

where we have explicitly isolated the index that corresponds to the electrostatic interaction. The above expression can be integrated between arbitrary position a and b (e.g., the position of the interface and infinity) along the z direction,

$$\int_a^b \chi^{(3)}_{ijk,\perp}E_{\mathrm{dc},\perp}(z)dz = \chi^{(3)}_{ijk,\perp}[\Phi(a)-\Phi(b)] \qquad (23)$$

so that the third-order signal is proportional to a potential difference.[24] Figure 3(a) shows a cartoon of this process: both the water molecules at the interface and other moieties present (i.e., adsorbents or constituents of the phase water is in contact with) generate a second-order signal. The electrostatic field that projects into the bulk generates a third-order signal proportional to the surface potential by reorienting water molecules and by regular third-order interactions.

TABLE II. Overview of the different contributions to the surface-selective ($\boldsymbol{\chi}^{(2)}$) and bulk-allowed ($\boldsymbol{\chi}^{(3)}$) signal near a charged water interface.

	Surface signal ($\boldsymbol{\chi}^{(2)}$)	Reorientation ($\boldsymbol{\chi}^{(3)}$)	Bulk signal ($\boldsymbol{\chi}^{(3)}$)
Molecular origin	$\boldsymbol{\beta}^{(2)}$	$m_{\mathrm{dc}}\boldsymbol{\beta}^{(2)}$	$\boldsymbol{\beta}^{(3)}$
$\chi_1^{(n)}$	$\neq 0 (\propto w_3)$	0	0
Origin	Interface	Bulk	Bulk

3. Distinguishing $\boldsymbol{\chi}^{(2)}$ and $\boldsymbol{\chi}^{(3)}$

Both the process proportional to $\boldsymbol{\beta}^{(2)}$ and the one proportional to $\boldsymbol{\beta}^{(3)}$ take place on the same length scale. The contribution scaling with $\boldsymbol{\beta}^{(2)}$ arises from the full bulk over which an electrostatic field is present. The electrostatic orientation effect is explicitly *not* limited to a few ordered layers where the electrostatic field is strong but rather is very subtle throughout the bulk. To give an example, at low local-field strength (e.g., $m_{\mathrm{dc}}\,E_{\mathrm{dc}} \approx 10^{-4}$) a $\boldsymbol{\beta}^{(2)}$ contribution to $\boldsymbol{\chi}^{(3)}$ may be the result of one in a thousand molecules that are actually oriented. Since such a subtle reorientation will likely not change the properties of the bulk much, the $\boldsymbol{\beta}^{(2)}$ that is probed is that of bulk water.

It follows from Eqs. (10) and (16) that both contributions to $\boldsymbol{\chi}^{(3)}$ obey the same symmetry rule $\chi_1^{(3)} = \chi^{(3)}_{\perp\perp\perp,\perp} - \chi^{(3)}_{\|\|\|\perp,\perp} - \chi^{(3)}_{\|\perp\|,\perp} - \chi^{(3)}_{\perp\|\|,\perp} = 0$. The direct consequence of this symmetry is that the overall value of $\chi_1^{(3)}$ is zero. The contributions that scale with $\boldsymbol{\beta}^{(2)}$ and $\boldsymbol{\beta}^{(3)}$ can, therefore, not be distinguished by testing the value of different $\boldsymbol{\chi}^{(3)}$ elements. It is possible, however, to compare the relative values of $\boldsymbol{\beta}^{(2)}$ and $\boldsymbol{\beta}^{(3)}$ by varying the sample temperature[24] since m_{dc} is temperature dependent.

In general, it is possible to distinguish the surface signal ($\boldsymbol{\chi}^{(2)}$) of a moiety present at the interface from the bulk signal ($\boldsymbol{\chi}^{(3)}$) by comparing the values of $\chi_1^{(2)}$ and $\chi_1^{(3)}$. By symmetry, $\chi_1^{(3)}$ is necessarily equal to 0 while no such limitation exists for $\chi_1^{(2)}$. Table II summarizes the different molecular origins of contributions to second- and third-order signals.

III. NONLINEAR LIGHT SCATTERING

In a scattering mode SH or SF generation experiment, the incoming pulses generate a nonlinear polarization at the surface of a particle in suspension, rather than at a planar interface. The nonlinear polarization varies in direction, phase, and magnitude across the particle surface. The coherent interference of the field between different points on a particle surface leads to an angular scattering pattern.

It is often convenient to resort to an effective particle susceptibility $\boldsymbol{\Gamma}^{(2)}$ that contains all information on scatterer geometry[53] so that the sum-frequency signal corresponds to

$$\mathbf{E}_0(\theta) \propto \boldsymbol{\Gamma}^{(2)}(\theta):\mathbf{E}_1\mathbf{E}_2. \tag{24}$$

For SH scattering, $\mathbf{E}_1=\mathbf{E}_2$. The effective susceptibility $\boldsymbol{\Gamma}^{(2)}$ is explicitly dependent on the scattering angle θ. Expressions for $\boldsymbol{\Gamma}^{(2)}$ have been derived for spherical[37,53,54] and cylindrical[56] particles. Here we will use expressions derived for spherical particles under the Rayleigh-Gans-Debye (RGD) approximation. The RGD approximation assumes, for all frequencies, a negligible difference between the indices of refraction of the components in a suspension. This approximation is valid for systems in which the relative index of refraction between solvent and particle is close to unity,[66] which is often the case for dielectrics. Moreover, for particles with a radius smaller than the sum-frequency or second-harmonic wavelength, the qualitative features of the scattering pattern are preserved.[67]

Figure 3(b) shows the scattering geometry for our model: two source waves with wave vectors $\mathbf{k}_1$ and $\mathbf{k}_2$ are incident on a particle. These waves are typically collinear and degenerate in a SH scattering experiment. In a SF scattering experiment, $\mathbf{k}_1$ and $\mathbf{k}_2$ differ in wave number and are incident with relative opening angle β. The emitted nonlinear signal is detected at an angle θ with respect to the forward direction defined by $\mathbf{k}_1+\mathbf{k}_2$ and has a wave vector $\mathbf{k}_0$. A scattering vector $\mathbf{q}$ is defined as the difference between scattering and forward directions $\mathbf{k}_0-\mathbf{k}_1-\mathbf{k}_2$. The angle between $\mathbf{k}_2$ and the forward direction, which is determined by the opening angle and the source frequencies, is denoted by α for convenience. We define a Cartesian laboratory coordinate frame with the z-axis lined up with the forward scattering direction. The components of $\boldsymbol{\chi}^{(2)}$ follow the curvature of the sphere, which defines the perpendicular ($\perp$) and ($\parallel$) directions (denoted in Fig. 3 as $\chi_\perp$ and $\chi_\parallel$). Finally, we need to choose a convenient coordinate frame for the effective susceptibility $\boldsymbol{\Gamma}^{(2)}$. The expression for $\boldsymbol{\Gamma}^{(2)}$ is simplified if this coordinate frame is aligned with the scattering vector $\mathbf{q}$. In that case, the effective susceptibility is[37,53,54]

$$\Gamma^{(2)}_{ijk} = \sum_{abc} \int_\Omega T_{ai}T_{bj}T_{ck}\chi^{(2)}_{abc}e^{i\mathbf{q}\cdot\mathbf{r}'}d\Omega. \tag{25}$$

The matrix T now represents the coordinate transform from the coordinate system of $\boldsymbol{\chi}^{(2)}$ [indices (a,b,c) to the coordinate system of $\boldsymbol{\Gamma}^{(2)}$ (indices (i,j,k)]. The integration is carried out over the entire surface Ω of the particle, $\mathbf{r}'$ is the position on this surface.

For a nonchiral, rotationally isotropic particle surface, the components of $\boldsymbol{\Gamma}^{(2)}$ reflect the symmetry of $\boldsymbol{\chi}^{(2)}$ so that only four independent nonvanishing components remain: $\Gamma^{(2)}_{\perp\perp\perp}$, $\Gamma^{(2)}_{\perp\parallel\parallel}$, $\Gamma^{(2)}_{\parallel\perp\parallel}$, and $\Gamma^{(2)}_{\parallel\parallel\perp}$ (similarly, $\Gamma^{(2)}_{\parallel\parallel\perp}=\Gamma^{(2)}_{\parallel\perp\parallel}$ for SH scattering). Here, $\perp(\parallel)$ again denote perpendicular and parallel orientation (denoted by $\Gamma_\perp$ and $\Gamma_\parallel$ in Fig. 3) but with respect to a virtual plane of which $\mathbf{q}$ is the normal vector, i.e., $\perp$ lies along $\mathbf{q}$ while $\parallel$ denotes any direction orthogonal to $\mathbf{q}$. Similar to the definition of $\chi^{(2)}_{1\ldots4}$ earlier, we define $\Gamma^{(2)}_{1\ldots4}$ as $\Gamma^{(2)}_1=\Gamma^{(2)}_{\perp\perp\perp}-\Gamma^{(2)}_{\perp\parallel\parallel}-\Gamma^{(2)}_{\parallel\perp\parallel}-\Gamma^{(2)}_{\parallel\parallel\perp}$, $\Gamma^{(2)}_2=\Gamma^{(2)}_{\perp\parallel\parallel}$, $\Gamma^{(2)}_3=\Gamma^{(2)}_{\parallel\perp\parallel}$, and $\Gamma^{(2)}_4=\Gamma^{(2)}_{\parallel\parallel\perp}$.

The relation between $\boldsymbol{\chi}^{(2)}$ and $\boldsymbol{\Gamma}^{(2)}$ depends on two scattering form factor functions $F_1(qR)$ and $F_2(qR)$. These are a function of the product of the norm of the scattering vector $\mathbf{q}$ and the particle radius R,

$$F_1(qR) = 2\pi IR^2\left[\frac{\sin(qR)}{(qR)^2} - \frac{\cos(qR)}{qR}\right], \tag{26}$$

$$F_2(qR) = 4\pi IR^2\left[3\frac{\sin(qR)}{(qR)^4} - 3\frac{\cos(qR)}{(qR)^3} - \frac{\sin(qR)}{(qR)^2}\right]. \tag{27}$$

The value of qR is related to the scattering angle by the relation $qR=2|\mathbf{k}_0|R\sin(\theta/2)$. We can write the relation between $\boldsymbol{\Gamma}^{(2)}$ and $\boldsymbol{\chi}^{(2)}$ as a matrix multiplication,

$$\begin{pmatrix}\Gamma^{(2)}_1\\ \Gamma^{(2)}_2\\ \Gamma^{(2)}_3\\ \Gamma^{(2)}_4\end{pmatrix} = \begin{pmatrix}2F_1-5F_2 & 0 & 0 & 0\\ F_2 & 2F_1 & 0 & 0\\ F_2 & 0 & 2F_1 & 0\\ F_2 & 0 & 0 & 2F_1\end{pmatrix}\begin{pmatrix}\chi^{(2)}_1\\ \chi^{(2)}_2\\ \chi^{(2)}_3\\ \chi^{(2)}_4\end{pmatrix}, \tag{28}$$

where $\chi^{(2)}_1=\chi^{(2)}_{\perp\perp\perp}-\chi^{(2)}_{\perp\parallel\parallel}-\chi^{(2)}_{\parallel\perp\parallel}-\chi^{(2)}_{\parallel\parallel\perp}$, $\chi^{(2)}_2=\chi^{(2)}_{\perp\parallel\parallel}$, $\chi^{(2)}_3=\chi^{(2)}_{\parallel\perp\parallel}$, and $\chi^{(2)}_4=\chi^{(2)}_{\parallel\parallel\perp}$ and the components $\Gamma^{(2)}_{1\ldots4}$ follow the same dependence on the corresponding $\boldsymbol{\Gamma}^{(2)}$ components. The reordering that leads to the $\chi^{(2)}_1$ and $\Gamma^{(2)}_1$ components not only simplifies the above matrix, but also the expression for the eventual scattered field. In the case of SF scattering, these are

$$E_{ppp} \propto \cos\left(\frac{\theta}{2}\right)\cos\left(\frac{\theta}{2}-\alpha\right)\cos\left(\frac{\theta}{2}-\alpha+\beta\right)\Gamma^{(2)}_1 + \cos(\theta-\alpha+\beta)E_{ssp} + \cos(\theta-\alpha)E_{sps} + \cos(\beta)E_{pss}, \tag{29}$$

$$E_{ssp} \propto \cos\left(\frac{\theta}{2}-\alpha\right)\Gamma^{(2)}_2, \tag{30}$$

$$E_{sps} \propto \cos\left(\frac{\theta}{2}-\alpha+\beta\right)\Gamma^{(2)}_3, \tag{31}$$

$$E_{pss} \propto \cos\left(\frac{\theta}{2}\right)\Gamma^{(2)}_4, \tag{32}$$

where the indices $p(s)$ denote electric field polarizations parallel (perpendicular) to the (x,z) laboratory plane. In the case of SH scattering, these expressions reduce to

$$E_{pp} \propto \cos^3\left(\frac{\theta}{2}\right)\Gamma^{(2)}_1 + 2\cos(\theta)\cos\left(\frac{\theta}{2}\right)\Gamma^{(2)}_2 + E_{ps}, \tag{33}$$

$$E_{ps} \propto \cos\left(\frac{\theta}{2}\right)\Gamma^{(2)}_4 \tag{34}$$

with $E_{pp}(E_{ps})$ the p-in/p-out (s-in/p-out) SH signal.

NLS from the third-order contribution

It is possible to determine the scattering pattern originating from the bulk $\boldsymbol{\chi}^{(3)}$ contribution. Similar to the $\boldsymbol{\Gamma}^{(2)}$ tensor

we can determine the value of the $\mathbf{\Gamma}^{(3)}$ tensor. The electrostatic field always points in the radial direction of the particle and does not depend on the external electromagnetic probing fields. It therefore makes sense to absorb the geometrical effects of this radial field into the properties of $\mathbf{\Gamma}^{(3)}$, which then becomes a tensor of the same rank as $\mathbf{\Gamma}^{(2)}$,

$$\Gamma_{ijk}^{(3)} = \sum_{abc} \int_R^\infty \int_\Omega T_{ai} T_{bj} T_{ck} \chi_{abc}^{(3)} e^{i\mathbf{q}\cdot\mathbf{r}} d\Omega dr. \tag{35}$$

The electrostatic field always points along the normal direction of the particle surface, and therefore does not influence the integral. The remaining integral over the angular range Ω is then identical to that of Eq. (25), and evaluates to the same linear combinations of F_1 and F_2. Because of the symmetry properties of $\boldsymbol{\chi}^{(3)}$, however, the value of $\chi_1^{(3)} = \chi_{\perp\perp\perp,\perp}^{(3)} - \chi_{\parallel\parallel\perp,\perp}^{(3)} - \chi_{\parallel\perp\parallel,\perp}^{(3)} - \chi_{\perp\parallel\parallel,\perp}^{(3)}$ vanishes. As a result, $\Gamma_1^{(3)}$ vanishes. The resulting scattering pattern for the $\boldsymbol{\chi}^{(3)}$ processes is therefore fixed, save for the relative values of $\Gamma_{2,3,4}^{(3)}$ and the trigonometric terms arising from Eq. (32). For $\boldsymbol{\chi}^{(3)}$-SF scattering they become

$$E_{ppp} \propto \cos(\theta - \alpha + \beta) E_{ssp} + \cos(\theta - \alpha) E_{sps} + \cos(\beta) E_{pss}, \tag{36}$$

$$E_{ssp} \propto \cos\left(\frac{\theta}{2} - \alpha\right) \Gamma_2^{(3)}, \tag{37}$$

$$E_{sps} \propto \cos\left(\frac{\theta}{2} - \alpha + \beta\right) \Gamma_3^{(3)}, \tag{38}$$

$$E_{pss} \propto \cos\left(\frac{\theta}{2}\right) \Gamma_4^{(3)} \tag{39}$$

while for SH scattering they are

$$E_{pp} \propto 2\cos(\theta)\cos\left(\frac{\theta}{2}\right) \Gamma_2^{(3)} + E_{ps}, \tag{40}$$

$$E_{ps} \propto \cos\left(\frac{\theta}{2}\right) \Gamma_4^{(3)}. \tag{41}$$

Polarization directions $p(s)$ are defined as perpendicular (parallel) to the plane of scattering, i.e., the plane in which $\mathbf{k}_{0,1,2}$ all lie. Each of the remaining three $\mathbf{\Gamma}^{(3)}$ components follows a simple relation that is dependent only on the scattering function F_1,

$$\Gamma_n^{(3)} = F_1(qR) \chi_n^{(3)} \Phi \quad (n = 2,3,4). \tag{42}$$

Figures 4(a) and 4(b) show simulations of the scattering patterns for SF and SH scattering from a particle of 500 nm radius. The components of $\boldsymbol{\chi}^{(3)}$ were set to $\chi_1^{(3)}=0$ and $\chi_{2,3,4}^{(3)}=0.33$, which are the values for water in the case of Kleinmann symmetry.[64]

Even though Kleinmann symmetry generally fails in practical cases,[68] assuming the symmetry holds will only induce small deviations from reality. Since the relative values of $\chi_{2,3,4}^{(3)}$ are not known *a priori*, we use the current values as a general description.

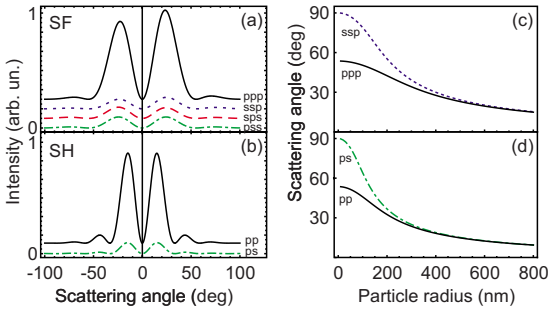

FIG. 4. (Color online) Angular scattering patterns of the $\boldsymbol{\chi}^{(3)}$ contribution to the nonlinear signal. Scattering patterns were simulated for $R=500$ nm particles, for four different polarizations [from top to bottom, (a) for SF scattering *ppp*, *ssp*, *sps*, and *pss* and (b) for SH scattering *pp* and *ps*]. For all other polarization combinations the signal vanishes. (a) shows SF scattering, with incoming beams of $\lambda_1=800$ nm and $\lambda_2=3447$ nm under a relative angle of $\beta=15°$. (b) SH show SH scattering for a fundamental beam of wavelength $\lambda=800$ nm. In both graphs, curves were offset for clarity. The third-order signal at *ppp* and *pp* polarizations is always dominant over that of other polarizations, both for SF and SH scattering. The position of the first maximum of the scattering pattern was also for (c) SF scattering and (d) SH scattering as a function of particle radius. As the particle radius increases, the maximum moves toward lower scattering angles.

In the SF case, source wavelengths are 800 and 3447 nm for the visible and infrared pulses, at a relative angle of $\beta=15°$. In the SH case, the fundamental wavelength is 800 nm. In both cases, the signal in the *ppp*/*pp* polarization is dominant over the signals in any of the other polarizations.

Since the scattering pattern shows a fixed shape, we can calculate the position of the first intensity maximum as a function of particle size. Figures 4(c) and 4(d) show the position of the first scattering maximum for SF scattering [Fig. 4(c)] and for SH scattering [Fig. 4(d)]. For small particle size, this maximum appears at 90° [*ssp* or *s*(in)-*p*(out) polarization] or 60° [*ppp* or *p*(in)-*p*(out) polarization], and progressively shift to lower scattering angles as the particle size increases. The $\boldsymbol{\chi}^{(2)}$ components for surface scattering, however, are not subject to the constraint $\chi_1^{(2)}=0$ (whereas $\chi_1^{(3)}=0$) and may lead to significantly different scattering patterns.

Figure 5 shows the difference in angular scattering pattern between the $\boldsymbol{\chi}^{(3)}$ contribution (solid lines) and the $\boldsymbol{\chi}^{(2)}$ contribution (dashed lines) for 500 nm particles with susceptibility values $\chi_1^{(2)}=1$, $\chi_{2,3,4}^{(2)}=0$, and $\chi_{2,3,4}^{(3)}=0.33$. Because the third-order contribution is dependent only on $F_1(qR)$, the angular scattering pattern of this contribution always shows a node at $qR=4.5$ (55° for 500 nm particles). Choosing this detection angle therefore minimizes the third-order signal. Similarly, the ratio of second-order to third-order signal can be tuned by adjusting the detection angle. For 500 nm particles, the maximum signal intensity for the third-order contribution is reached at 24°, an angle at which the second-order signal is also rather high. In our example, the second-order *ppp* contribution shows a minimum at 45°, whereas the *ssp* contribution shows a minimum at 63°. Choosing either of these angles maximizes the third-order to second-order signal ratio.

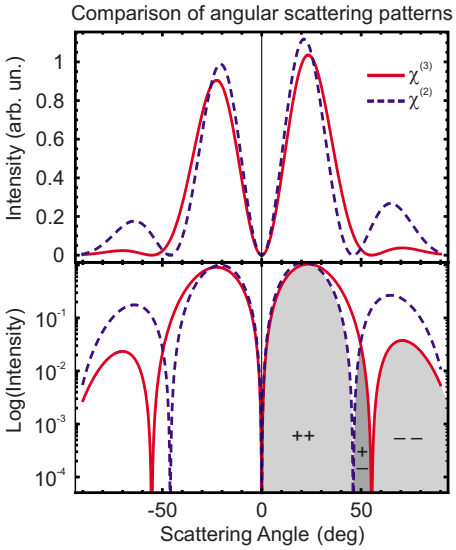

FIG. 5. (Color online) Comparison of the second-order (blue, dashed curve) and third-order (red, solid curve) SF scattering patterns of a particle with 500 nm radius and $\chi^{(2)}_1=1$, $\chi^{(2)}_{2,3,4}=0$, and $\chi^{(3)}_{2,3,4}=0.33$, for source waves of wavelength $\lambda_1=800$ nm and $\lambda_2=3447$ nm and opening angle 15°. The top panel shows the scattering patterns for the *ppp* polarization while the bottom panel shows the same scattering patterns on a logarithmic scale. The shaded areas indicate zones where the signs of the detected signals are the same (++ and −−) or opposite (+−). The third-order scattering pattern, for this particle size, always shows a node at 55°, whereas the second-order scattering pattern shows a more complicated behavior.

Because both the second- and third-order contributions are generated at or near the same interface, they interact coherently. The shaded areas in the bottom panel of Fig. 5 indicate the relative signs of the both signals, either both positive (++), both negative (−−) or of opposite amplitudes (+−). A change in relative sign between two resonant peaks or between a resonant peak and a broad background can lead to large changes in spectral signature.[69,70] A change in scattering angle that reverses the relative sign of second- and third-order contributions should therefore lead to a significant change in spectral signature.

IV. CONCLUSION

In summary, we have treated the molecular origin of second- and third-order signals in relation to a charged water interface. We have shown that the interaction of two source fields and the electrostatic field near the interface may give rise to a surface contribution and a bulk contribution. The surface contribution is a pure second-order process while the third-order bulk contribution consists of a pure third-order contribution and a second-order contribution due to molecular reorientation, induced by the electrostatic field. Since both of the bulk contributions depends linearly on all three input fields, they may both be regarded as third-order contributions. Both of these contributions are generated over the same length scale. Furthermore, the similar symmetry properties of the two third-order contribution make them indistinguishable.

We have derived the angular nonlinear light scattering pattern a third-order bulk interaction, and compared it to the angular scattering pattern from a second-order surface interaction. In contrast to the scattering pattern from a $\boldsymbol{\chi}^{(2)}$ process, which generally depends on the structure of the particle interface, the scattering pattern from the third-order contribution is fixed for a given solvent and particle size.

The fixed nature of the angular scattering pattern offers an advantage over reflection mode sum-frequency and second-harmonic experiments. Since typically the second-order and third-order contributions are recorded simultaneously, we can exploit the differences in angular scattering pattern to change the ratio between second-order and third-order signals. By measuring at the right scattering angles, the third-order contribution can be maximized, minimized or optimized with respect to the second-order signal. Therefore, by exploiting the additional degree of freedom the angular scattering pattern provides, it is possible to separate second- and third-order contributions, which is not possible in a reflection mode experiment.

ACKNOWLEDGMENTS

This work is part of the research program of the Max Planck Society. Additional funding was received from the German Science Foundation (DFG) under Contract No. 560398 and the European Research Council (ERC) under Contract No. 240556. R.K.C. received additional funding from the European Commission (FP7) under Contract No. 220505.

*debeer@mf.mpg.de
†roke@mf.mpg.de

[1] R. J. Hunter, *Foundations of Colloid Science* (Oxford University Press, Oxford, 2002).
[2] T. F. Heinz, *Nonlinear Surface Electromagnetic Phenomena* (Elsevier, New York, 1991), Chap. 5, p. 353.
[3] Y. R. Shen, Nature (London) **337**, 519 (1989).
[4] J. F. McGilp, J. Phys.: Condens. Matter **2**, 7985 (1990).
[5] Y. R. Shen, Surf. Sci. **299**, 551 (1994).
[6] C. D. Bain, J. Chem. Soc., Faraday Trans. **91**, 1281 (1995).
[7] K. B. Eisenthal, Chem. Rev. **96**, 1343 (1996).
[8] N. Bloembergen, Appl. Phys. B: Lasers Opt. **68**, 289 (1999).
[9] M. J. Shultz, C. Schnitzer, D. Simonelli, and S. Baldelli, Int. Rev. Phys. Chem. **19**, 123 (2000).
[10] G. L. Richmond, Annu. Rev. Phys. Chem. **52**, 357 (2001).
[11] M. J. Shultz, S. Baldelli, C. Schnitzer, and D. Simonelli, J. Phys.

Chem. B **106**, 5313 (2002).
[12] Z. Chen, Y. R. Shen, and G. A. Somorjai, Annu. Rev. Phys. Chem. **53**, 437 (2002).
[13] G. L. Richmond, Chem. Rev. **102**, 2693 (2002).
[14] S. Sioncke, T. Verbiest, and A. Persoons, Mater. Sci. Eng. R. **42**, 115 (2003).
[15] G. J. Simpson, ChemPhysChem **5**, 1301 (2004).
[16] M. B. Raschke and Y. R. Shen, Curr. Opin. Solid State Mater. Sci. **8**, 343 (2004).
[17] M. A. Belkin and Y. R. Shen, Int. Rev. Phys. Chem. **24**, 257 (2005).
[18] A. G. Lambert, P. B. Davies, and D. J. Neivandt, Appl. Spectrosc. Rev. **40**, 103 (2005).
[19] F. Vidal and A. Tadjeddine, Rep. Prog. Phys. **68**, 1095 (2005).
[20] C. H. Lee, R. K. Chang, and N. Bloembergen, Phys. Rev. Lett. **18**, 167 (1967).
[21] B. F. Levine and C. G. Bethea, J. Chem. Phys. **63**, 2666 (1975).
[22] X. L. Zhao, S. Subrahmanyan, and K. B. Eisenthal, Chem. Phys. Lett. **171**, 558 (1990).
[23] A. Castro, K. Bhattacharyya, and K. B. Eisenthal, J. Chem. Phys. **95**, 1310 (1991).
[24] S. W. Ong, X. L. Zhao, and K. B. Eisenthal, Chem. Phys. Lett. **191**, 327 (1992).
[25] X. L. Zhao, S. W. Ong, and K. B. Eisenthal, Chem. Phys. Lett. **202**, 513 (1993).
[26] X. L. Zhao, S. W. Ong, H. F. Wang, and K. B. Eisenthal, Chem. Phys. Lett. **214**, 203 (1993).
[27] F. M. Geiger, Annu. Rev. Phys. Chem. **60**, 61 (2009).
[28] H. Wang, E. C. Y. Yan, E. Borguet, and K. B. Eisenthal, Chem. Phys. Lett. **259**, 15 (1996).
[29] H. F. Wang, E. C. Y. Yan, Y. Liu, and K. B. Eisenthal, J. Phys. Chem. B **102**, 4446 (1998).
[30] A. Srivastava and K. B. Eisenthal, Chem. Phys. Lett. **292**, 345 (1998).
[31] E. C. Y. Yan and K. B. Eisenthal, J. Phys. Chem. B **103**, 6056 (1999).
[32] E. C. Y. Yan and K. B. Eisenthal, Biophys. J. **79**, 898 (2000).
[33] N. Yang, W. E. Angerer, and A. G. Yodh, Phys. Rev. Lett. **87**, 103902 (2001).
[34] Y. Jiang, P. T. Wilson, M. C. Downer, C. W. White, and S. P. Withrow, Appl. Phys. Lett. **78**, 766 (2001).
[35] X. M. Shang, Y. Liu, E. Yan, and K. B. Eisenthal, J. Phys. Chem. B **105**, 12816 (2001).
[36] K. B. Eisenthal, Chem. Rev. **106**, 1462 (2006).
[37] S. Roke, W. G. Roeterdink, J. E. G. J. Wijnhoven, A. V. Petukhov, A. W. Kleyn, and M. Bonn, Phys. Rev. Lett. **91**, 258302 (2003).
[38] S. Roke, J. Buitenhuis, J. C. van Miltenburg, M. Bonn, and A. van Blaaderen, J. Phys.: Condens. Matter **17**, S3469 (2005).
[39] S. Roke, O. Berg, J. Buitenhuis, A. van Blaaderen, and M. Bonn, Proc. Natl. Acad. Sci. U.S.A. **103**, 13310 (2006).
[40] J. I. Dadap, H. B. de Aguiar, and S. Roke, J. Chem. Phys. **130**, 214710 (2009).
[41] S. Roke, ChemPhysChem **10**, 1380 (2009).
[42] H. B. de Aguiar, A. G. F. de Beer, M. L. Strader, and S. Roke, J. Am. Chem. Soc. **132**, 2122 (2010).
[43] E. C. Y. Yan, Y. Liu, and K. B. Eisenthal, J. Phys. Chem. B **102**, 6331 (1998).
[44] Y. Liu, C. Y. Yan, X. L. Zhao, and K. B. Eisenthal, Langmuir **17**, 2063 (2001).
[45] Y. Liu, E. C. Y. Yan, and K. B. Eisenthal, Biophys. J. **80**, 1004 (2001).
[46] J. Shan, J. I. Dadap, I. Stiopkin, G. A. Reider, and T. F. Heinz, Phys. Rev. A **73**, 023819 (2006).
[47] S. H. Jen and H. L. Dai, J. Phys. Chem. B **110**, 23000 (2006).
[48] S. H. Jen, G. Gonella, and H. L. Dai, J. Phys. Chem. A **113**, 4758 (2009).
[49] S. H. Jen, H. L. Dai, and G. Gonella, J. Phys. Chem. C **114**, 4302 (2010).
[50] A. G. F. de Beer and S. Roke, J. Chem. Phys. **132**, 234702 (2010).
[51] J. I. Dadap, J. Shan, K. B. Eisenthal, and T. F. Heinz, Phys. Rev. Lett. **83**, 4045 (1999).
[52] J. I. Dadap, J. Shan, and T. F. Heinz, J. Opt. Soc. Am. B **21**, 1328 (2004).
[53] S. Roke, M. Bonn, and A. V. Petukhov, Phys. Rev. B **70**, 115106 (2004).
[54] A. G. F. de Beer and S. Roke, Phys. Rev. B **75**, 245438 (2007).
[55] Y. Pavlyukh and W. Hubner, Phys. Rev. B **70**, 245434 (2004).
[56] J. I. Dadap, Phys. Rev. B **78**, 205322 (2008).
[57] A. G. F. de Beer, S. Roke, and J. I. Dadap (unpublished).
[58] D. A. Varshalovich, A. N. Moskalev, and V. K. Khersonskii, *Quantum Theory of Angular Momentum* (World Scientific, Singapore, 1988).
[59] J. Jerphagnon, Phys. Rev. B **2**, 1091 (1970).
[60] J. A. R. Coope, F. R. Snider, and R. F. McCourt, J. Chem. Phys. **43**, 2269 (1965).
[61] B. Dick, Chem. Phys. **96**, 199 (1985).
[62] H. F. Wang, W. Gan, R. Lu, Y. Rao, and B. H. Wu, Int. Rev. Phys. Chem. **24**, 191 (2005).
[63] G. J. Simpson and K. L. Rowlen, J. Am. Chem. Soc. **121**, 2635 (1999).
[64] R. W. Boyd, *Nonlinear Optics* (Academic, New York, 1992).
[65] D. S. Chemla and R. Bonneville, J. Chem. Phys. **68**, 2214 (1978).
[66] A. G. F. de Beer and S. Roke, Phys. Rev. B **79**, 155420 (2009).
[67] A. G. F. de Beer, H. B. de Aguiar, J. F. W. Nijsen, and S. Roke, Phys. Rev. Lett. **102**, 095502 (2009).
[68] C. A. Dailey, B. J. Burke, and G. J. Simpson, Chem. Phys. Lett. **390**, 8 (2004).
[69] L. F. Scatena and G. L. Richmond, J. Phys. Chem. B **108**, 12518 (2004).
[70] M. Sovago, E. Vartiainen, and M. Bonn, J. Phys. Chem. C **113**, 6100 (2009).